1	Human Activities Caused Hypoxia Expansion in a Large Eutrophic
2	<b>Estuary: Non-negligible Role of Riverine Suspended Sediments</b>
3	
4	Yue Nan <sup>1</sup> , Zheng Chen <sup>2</sup> , Bin Wang <sup>3</sup> , Bo Liang <sup>4</sup> , Jiatang Hu <sup>1,5,6*</sup>
5	
6	<sup>1</sup> School of Environmental Science and Engineering, Sun Yat-Sen University,
7	Guangzhou, 510275, China
8	<sup>2</sup> Earth, Ocean and Atmospheric Sciences Thrust, The Hong Kong University of
9	Science and Technology (Guangzhou), Guangzhou, 511455, China
10	<sup>3</sup> Department of Oceanography, Dalhousie University, Halifax, Nova Scotia, Canada
11	<sup>4</sup> Eco-Environmental Monitoring and Research Center, Pearl River Valley and South
12	China Sea Ecology and Environment Administration, Ministry of Ecology and
13	Environment of the People's Republic of China, Guangzhou, 510611, China
14	<sup>5</sup> Guangdong Provincial Key Laboratory of Environmental Pollution Control and
15	Remediation Technology, Guangzhou, 510275, China
16	<sup>6</sup> Southern Marine Science and Engineering Guangdong Laboratory (Zhuhai), Zhuhai
17	519000, China
18	
19 20	Correspondence: Jiatang Hu (hujtang@mail.sysu.edu.cn)

#### 21 Abstract

22

23

24

25

26

27

28

29

30

31

32

33

34

35

36

37

38

39

40

41

42

43

44

45

46

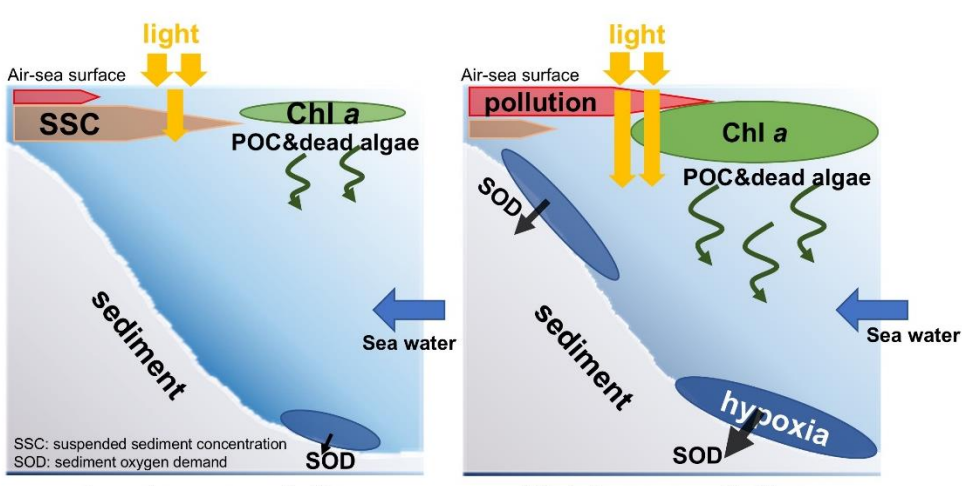
47

48

Increase in riverine nutrient loads was generally recognized as the primary cause of coastal deoxygenation, whereas the role of other riverine factors, especially suspended sediments, has received less attention. This study aims to discern the impacts of anthropogenic alterations in various riverine inputs on the subsurface deoxygenation over the past three decades in a large river-dominated estuary, the Pearl River Estuary (PRE). Using a physical-biogeochemical model, we reproduced the observed dissolved oxygen (DO) conditions off the PRE in the historical period (the 1990s with high suspended sediments concentration (SSC), high DO, and low nutrients) and the present period (the 2010s with low SSC, low DO, and high nutrients). In the 2010s, the PRE exhibited more extensive and persistent summer hypoxia, with the low oxygen area (DO < 4 mg/L) expanding by  $\sim$ 148% (to  $\sim$ 2926 km<sup>2</sup>) and the hypoxia area (DO < 3 mg/L) increasing by 192% (to ~617 km<sup>2</sup>). Low-oxygen durations extended to 15-35 days, and three distinct hypoxic centers formed under different controlling factors. Single-factor experiments suggested that decreased riverine DO content (46%) alone expanded low-oxygen areas in the upper estuarine regions by 44%, the decreased SSC (by 60%) alone cause a 47% expansion in the lower reach of PRE, and the increased nutrients alone (100% in dissolved inorganic nitrogen and 225% in phosphate) drove a 31% expansion. In comparison, the combined nutrient increases and the SSC declines synergistically enhanced primary production and bottom oxygen consumptions (dominated by sediment oxygen uptake), amplifying low-oxygen (104%) and hypoxic (192%) area growth in lower estuaries. Our results revealed that SSC declines, by improving light availability for productivity, play a larger role than nutrient increases in exacerbating deoxygenation off the PRE. This synergy complicates hypoxia mitigation efforts focused solely on nutrient controls. Given the widespread global declines in riverine suspended sediments, our findings underscore the importance for incorporating sediment-mediated processes, a relatively overlooked factor, in coastal deoxygenation studies.

- **Key words:** Deoxygenation; suspended sediments; nutrient inputs; decadal changes;
- 50 Pearl River Estuary

# 51 Graphical Abstract



Low human activities

High human activities

#### 1. Introduction

Hypoxia emerges when dissolved oxygen (DO) concentration drops below 3 mg/L in aquatic systems. It is an undesirable phenomenon which can lead to a series of biological and ecological consequences, such as damaging the habitat for aquatic organisms and imposing detrimental effects on the ecosystem community structure (Diaz and Rosenberg, 2008; Roman et al., 2019). Due to the substantial impacts from human socioeconomic activities, coastal regions have become a hotspot for hypoxia (Breitburg et al., 2018; Pitcher et al., 2021). Moreover, long-term exacerbation of hypoxia with spatial expansion and increased frequency has been frequently reported in estuarine and coastal regions worldwide during the past decades, including the Baltic Sea (Carstensen et al., 2014), the northern Gulf of Mexico (Bianchi et al., 2010), Chesapeake Bay (Murphy et al., 2011), the Yangtze River Estuary (Chen et al., 2017), and the Pearl River Estuary (Hu et al., 2021).

Plenty of studies were conducted to reveal the mechanism of hypoxia formation

and evolution in coastal regions. It has been widely recognized that coastal deoxygenation is largely attributed to the eutrophication-driven production of organic matters (Su et al., 2017; Wang et al., 2016; Howarth et al., 2011), which sink to the subsurface waters and bottom sediments, leading to intense oxygen depletion (Wang et al., 2014; Hagy et al., 2005). This would induce hypoxia when the density stratification restricts DO replenishment from the surface waters (Wang et al., 2018; Murphy et al., 2011). One important reason underlying eutrophication and hypoxia is the excessive nutrients that are discharged into the water column and stimulate phytoplankton blooms (Cullen, 2015; Wang et al., 2021; Cormier et al., 2023). In addition, human activities, such as dam construction (Bussi et al., 2021) and soil-water conservation measures (Yang et al., 2024) can significantly reduce suspended sediment in estuaries. Hence, an improved light condition, e.g., due to the decreased suspended sediment loads, could also favor the enhancement of local production and hence hypoxia (Ge et al., 2020; Huang et al., 2022). The effects of nutrient and light conditions vary in coastal systems due to different hydrodynamic and topographic features, which makes the formulation of hypoxia mitigation strategies more challenging. Therefore, a quantitative assessment on the importance of these factors in generating hypoxia is crucial for understanding the primary drivers of hypoxia evolution and for proposing effective countermeasures. A case in point is the Pearl River Estuary (PRE), which is situated in the northern South China Sea and close to the Guangdong-Hong Kong-Macao Great Bay Area (Fig. 1a). Owing to the relatively large nutrient inputs and vertical stratification formed by freshwater plume, hypoxia typically occurs during summer in the bottom waters of the PRE. Before the 2000s, it was an episodic and small-scale issue because of the synergetic effect of shallow topography, high turbidity (Ma et al., 2022), and the intermittent stratification due to periodic disturbance by the tides. However, large-scale occurrences of low oxygen (when DO < 4 mg/L) and hypoxia were frequently reported in recent years. For example, it was estimated that the low-oxygen area within the PRE achieved 1000 km<sup>2</sup> and 1500 km<sup>2</sup> during summer in 2010 (Wen et al., 2020) and 2015

67

68

69

70

71

72

73

74

75

76

77

78

79

80

81

82

83

84

85

86

87

88

89

90

91

92

93

94

(Li et al., 2018), respectively, which were nearly double to that before the 2000s (Li et al., 2020). Hu et al. (2021) compiled historical observations over four decades to investigate the long-term deoxygenation trend and its spatial expansion in the PRE. They highlighted the significant contributions of increased nutrient and decreased sediment fluxes from the Pearl River to the exacerbation of low-oxygen conditions in the region. Besides, the low-oxygen inflows from the Pearl River could also contribute to the low-oxygen area in the upper estuary (Hu et al., 2021). Nevertheless, a quantitative understanding of their relative contributions to the low-oxygen expansion in the PRE is lacking, particularly in different subregions (Fig.1b) where the mechanisms controlling the low-oxygen conditions are different. In the upper part of the PRE (Lingdingyang waters), aerobic respiration of terrestrial organic matter plays a greater role (Su et al., 2017; Yu et al., 2020); in the downstream regions of the PRE, deoxygenation is primarily controlled by eutrophication (Yu and Gan, 2022; Chen et al., 2024).

In this study, we used a coupled physical-biogeochemical model to investigate the

In this study, we used a coupled physical-biogeochemical model to investigate the decadal changes (the 1990s versus the 2010s) in summertime DO contents and related biogeochemical processes in the PRE and to quantify the relative contributions of the changing riverine inputs (including nutrients, suspended sediments, and oxygen content; Fig. 1c-f) to the long-term expansion of low oxygen (DO < 4 mg/L) and hypoxia (DO < 3 mg/L) in the region.

# 2. Material and methods

## 2.1 Study area

The PRE and its adjacent shelf waters (Fig. 1a) represent an estuarine system under intensive human activities. One major anthropogenic impact in the PRE is the terrestrial substances fed by the Pearl River, which is the third largest river in China with an average annual runoff of  $3.26 \times 10^{11}$  m<sup>3</sup>/ Year (Luo et al., 2002), through eight river outlets, including Humen, Jiaomen, Hongqili, Hengmen, Modaomen, Jitimen,

Hutiaomen, and Yamen (Fig. 1a). The long-term DO and water quality data used here were collected from open sources (e.g. government websites) and published studies (detailed in Data availability and Table S1 of Supplement). Over the past few decades, the terrestrial inputs from the Pearl River have experienced remarkable changes in oxygen content, sediment loads, and nutrients including dissolved inorganic nitrogen (DIN) and dissolved inorganic phosphorus (DIP) (Fig. 1c-f). Consequently, the ecological environments of the PRE have changed significantly.

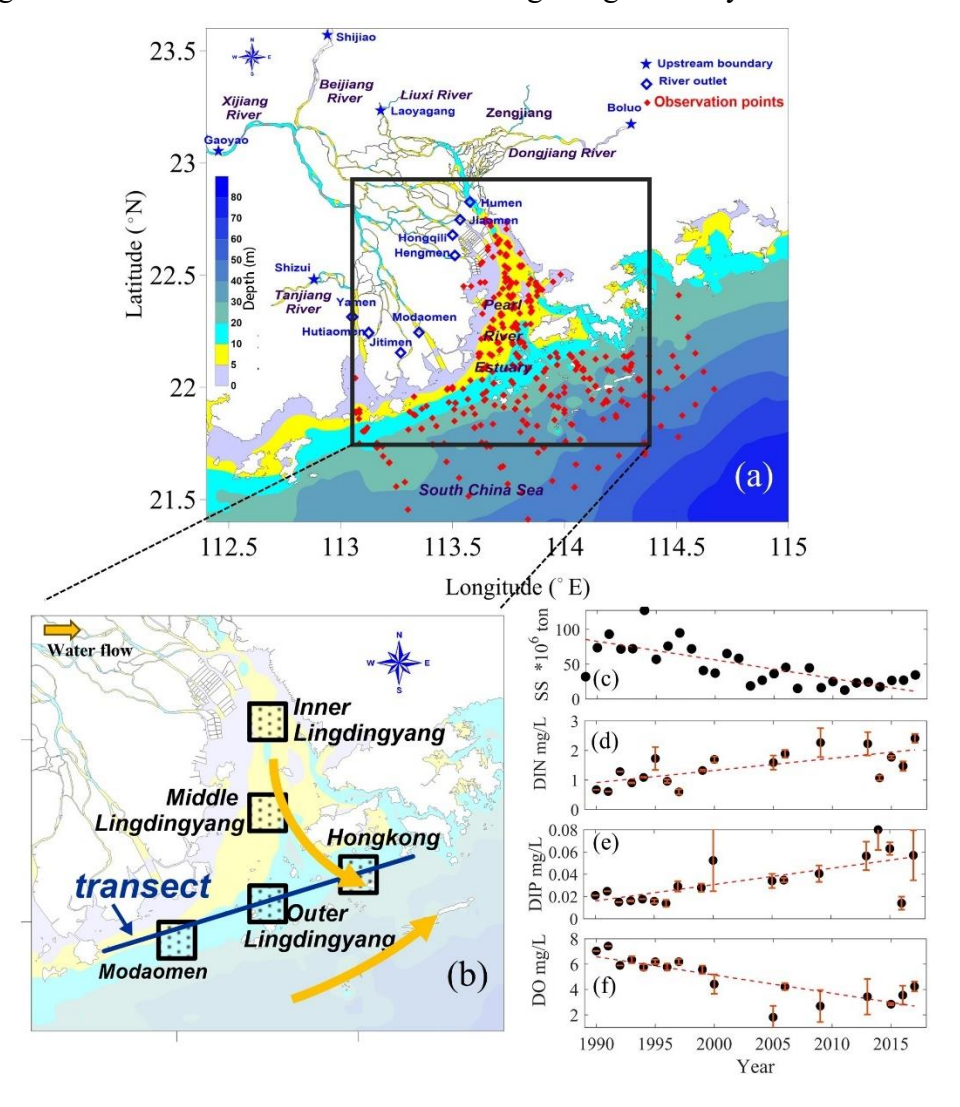


Fig. 1. (a) Study area of the PRE and sampling sites during 1985-2017; (b) Five subregions and a transect along the coastal transition zone used for analysis and the surface water flow direction; (c) Annual loads of suspended sediments (SS) from the Pearl River; (d-f) Summer-averaged (June to August) surface-layer (within the upper 2 m of water column) concentrations of nutrients (DIN, DIP) and dissolved oxygen (DO)

at Humen Outlet (the primary monitoring site). Error bars indicate intra-summer variability across sampling dates.

During the 1990s, the Pearl River Estuary (PRE) experienced low eutrophication levels, consistent with limited upstream urbanization and relatively high sediment loads. This period saw extensive construction of water infrastructure, mostly completed by 2000\_including over 8,636 reservoirs in the Pearl River Basin (Wu et al., 2016), which drove a significant decline in riverine suspended sediment concentration (SSC) (Zhang et al., 2008). After 2000, accelerated urbanization and continued hydraulic development further altered river inputs, with monitoring data showing decreased sediment loads (Fig. 1c) and increased nutrient concentrations (Fig. 1d–e). These changes collectively enhanced phytoplankton blooms potential, exacerbating eutrophication and hypoxia. These long-term variations of riverine substances have also been reported by Lai et al. (2022) and Hu et al. (2021). In the meantime, the oxygen content in the PRE has exhibited a notable drawdown with significant expansions in low-oxygen extents in recent summers (Fig. 2), which has been revealed by the cruise observations in the PRE (Li et al., 2021; Su et al., 2017; Hu et al., 2021; Lu et al., 2018).

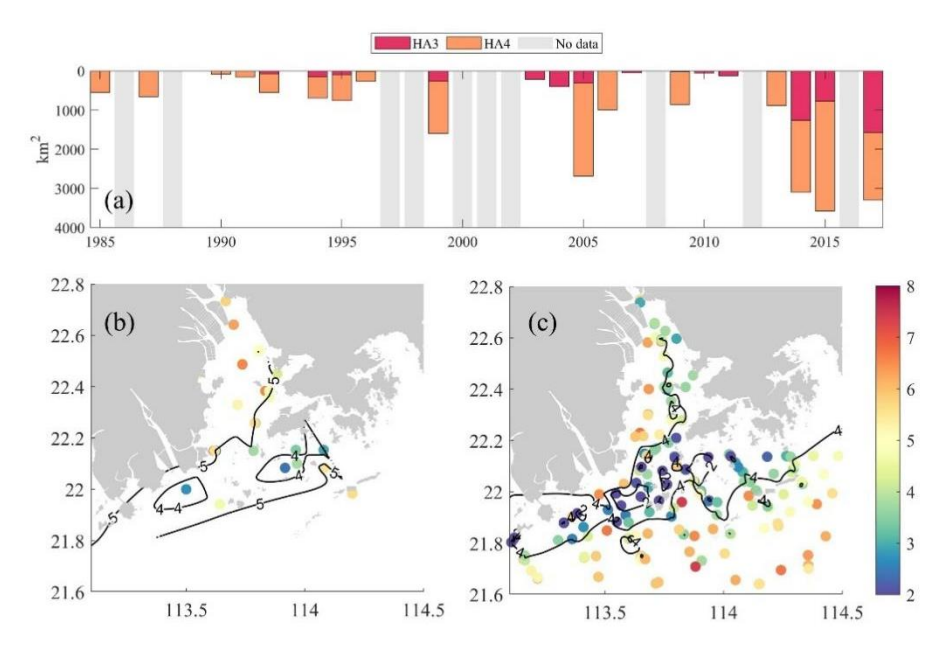


Fig. 2. (a) Interannual variations of low-oxygen area (HA4, DO < 4 mg/L) and hypoxic area (HA3, DO < 3 mg/L) in the bottom waters ( $\sim$ 1-2 m above sediments) of the PRE, calculated via liner interpolation on a 0.01° × 0.01° grid using summer cruise

observations (note that the grey patches indicate data gaps). Spatial distributions of summer-averaged bottom DO concentrations during (b) 1991-1996 and (c) 2013-2017.

## 2.2 Model settings and validation

157

158

159

160

161

162

163

164

165

166

167

168

169

170

171

172

173

174

175

176

177

178

179

180

181

182

183

184

#### 2.2.1 Model descriptions and settings

An online 1D-3D coupled physical-biogeochemical model, which has been extensively verified and applied in the PRE (Wang et al., 2017; Wang et al., 2018; Hu et al., 2011; Zhang et al., 2022), was utilized here to reproduce the oxygen dynamics under the long-term changes in riverine nutrients, suspended sediment concentration (SSC), and oxygen content (Fig. 1c-f). This 1D-3D modeling framework integrates a 1D representation of the Pearl River network with a 3D simulation of the Pearl River Estuary and adjacent shelf region, operating in an online coupling mode. The 1D component numerically solves the Saint-Venant equations using a Preissmann scheme, discretizing the river network into 299 sections with five upstream boundaries (specified as either discharge or water level inputs). The 3D component employs the ECOM model with 16 vertical layers and adaptive horizontal resolution (400m to 3km), forced by tides, atmospheric forcing, and open boundary conditions. The two components exchange fluxes at eight river outlets: the 3D model incorporates river discharge from the 1D model as upstream boundary conditions, while the 1D model uses water levels computed by the 3D model as its downstream boundaries at each time step. This 1D-3D modeling framework was initially developed to investigate nutrient fluxes to the PRE and has been extended and validated to simulate oxygen dynamics and hypoxia in the PRE (Wang et al., 2017; Wang et al., 2018; Hu et al., 2011; Zhang et al., 2022; Chen et al., 2024). For the sake of conciseness in the main text, detailed descriptions on the physical and suspended sediment modules were provided in the Supplement (Text S1). Regarding the biogeochemical module, it is based on the Row-Column Aesop (RCA), which simulates interactive cycles of oxygen, carbon, nitrogen, phosphorus, and silicon in the water column (HydroQual, 2004). The schemes for DO dynamics and phytoplankton growth in the model can be found in previous studies

- 185 (Wang et al., 2017; Wang et al., 2018). The nutrient limitation factor  $(G_N(N))$  is
- parameterized as:

187 
$$G_N(N) = Min\left(\frac{DIN}{K_{mN} + DIN}, \frac{DIP}{K_{mP} + DIP}, \frac{Si}{K_{mSi} + Si}\right)$$
(1)

- where DIN, DIP, and Si are concentrations (mg  $L^{-1}$ ) of dissolved inorganic nitrogen
- 189 (NO<sub>3</sub><sup>-</sup>, NH<sub>4</sub><sup>+</sup>), phosphorus (PO<sub>4</sub><sup>3-</sup>), and silicon (SiO<sub>3</sub><sup>2-</sup>), respectively.  $K_{mN}$ ,  $K_{mP}$ , and
- 190  $K_{mSi}$  are their corresponding half-saturation constants. A higher  $G_N(N)$  indicates
- weaker nutrient limitation. Given the stronger N and P limitation compared to Si in the
- 192 Pearl River Estuary (PRE), this study emphasizes N and P.
- 193 The light limitation factor  $G_I(I)$  is parameterized as:

194 
$$G_I(I) = \frac{e}{k_e H} \left[ \exp\left(\frac{-I_0(t)}{I_S} e^{-k_e H}\right) - \exp\left(\frac{-I_0(t)}{I_S}\right) \right]$$
 (2)

with the light extinction coefficient:

196 
$$k_e = k_{ebase} + k_c * a_{cchl} * P_c + k_{sed} * SSC + k_{POC} * POC$$
 (3)

and the surface light at depth:

198 
$$I_0 = I_{surf} * e^{-k_e * H}$$
 (4)

- Here, H is water depth (m),  $I_s$  the saturation light intensity (ly day<sup>-1</sup>),  $I_{surf}$  is the
- surface light (ly day<sup>-1</sup>), and the k-terms are light attenuation coefficients due to water,
- 201 Chl a, SSC, and POC.
- 202 To assess light conditions, the eutrophic depth H<sub>E</sub> is computed as the depth where light
- is 1% of surface intensity:

206

207

208

209

210

211

$$204 I_{surf} * e^{-k_e * H_E} = I_{surf} * 1\% (5)$$

205 A deeper  $H_E$  implies better light conditions for phytoplankton growth.

#### 2.2.2 Model validation

The coupled physical-biogeochemical model mentioned above has already been validated against a variety of observations for several periods, which showed good performance in reproducing the physical conditions, suspended sediment dynamics, and biogeochemical cycles in the PRE. We briefly summarized the validation results here. For the physical and suspended sediment modules, Hu and Li (2009) has applied

the 1D-3D coupled model to establish 30-day realistic simulations for July 1999 and February 2001. The simulated water levels, discharges, salinity, and SSC agreed well with the observations in the Pearl River network and the PRE for both periods, with correlation coefficients all greater than 0.65 in summer. The simulated SSC at the surface was also compared to satellite remote sensing data, which showed a fairly close spatial pattern and comparable concentration magnitude. Furthermore, Wang et al. (2017) provided an extensive model validation using field data collected from four seasonal cruises in 2006, with high correlations for water levels (> 0.95), salinity (> 0.90) and temperature (> 0.80) and low root-mean-standard-errors between the simulation and observations in summer. Then, the biogeochemical module was established and used to explore the nutrient and oxygen dynamics off the PRE in July 1999 and January-December 2006 (Hu and Li, 2009; Wang et al., 2017). Detailed model settings and parameters can be found in Wang et al. (2017). For validation, comparisons with the water quality data from cruise surveys indicated that the biogeochemical module was robust to reproduce the spatial distributions of nutrient, chlorophyll a, and oxygen concentrations in the PRE (Figs. 3, 5). To further assess light attenuation dynamics, we obtained diffuse attenuation coefficient at 490 nm (K<sub>d</sub>(490)) data for the PRE from the EUMETSAT Ocean color Thematic Assembly Centre (https://www.oceancolour.org/). We converted K<sub>d</sub>(490) to photosynthetically active radiation attenuation coefficient (K<sub>par</sub>) using the empirical formula proposed by Lee et al. (2005), and then calculated the euphotic depth using Eq. 5 in Section 2.2.1. Model-simulated and satellite-derived euphotic depths show close agreement in both the 1990s and 2010s (Fig. 4b, d), demonstrating consistent model performance across decades. For hypoxia simulation, the model accurately captured the observed temporal expansion of hypoxia, transitioning from localized bottom hypoxia in the 1990s (Fig. 2b-c) to widespread occurrences in the 2010s (Fig. 5d-e). Initial validation against

212

213

214

215

216

217

218

219

220

221

222

223

224

225

226

227

228

229

230

231

232

233

234

235

236

237

238

239

1994-1999 summer observations showed close agreement, with simulated low-oxygen

(HA4=1179.7 km²) and hypoxic (HA3=211.3 km²) areas matching observational estimates (802±437 km² and 131±84 km²; Fig. 2a, Table 3). For the 2013-2017 period, the model successfully replicated hypoxia intensification, as evidenced by HA4 expansion to 2925.5 km² aligning with observed 2715±1068 km². For the 2010s, simulated HA3 doubled to 617.2 km², consistent with observational uncertainty ranges (901±591 km²; 2013-2017 data). These results collectively confirm the model's robustness in simulating both historical patterns and emerging hypoxia dynamics. In addition, Wang et al. (2017) has compared the simulated oxygen kinetic terms (including the air-sea re-aeration rate, water-column respiration and production rates, and sediment oxygen demand) with observations in summer, which demonstrated the model's capability in representing the important oxygen source-sink processes (e.g., oxygen consumptions across the sediment-water interface) in the PRE. Detailed model settings and parameters can be found in Wang et al. (2017).

# 2.3 Model experiments

Based on the well-validated model run in 2006 (Wang et al., 2017), the present study performed diagnostic simulations for two representative periods, characterized by low nutrients and high suspended sediments and oxygen content during 1991-1996 (referring as to the "1990s case"; Table 1) versus high nutrients and low suspended sediments and oxygen content during 2013-2017 (referring as to the "2010s case"). Each case was run from 1 January to 31 August, driven by climatological physical conditions (freshwater discharges and wind speeds detailed in Text S1 of the Supplement) averaged over 1990-2017 and by mean observed values of riverine water quality components in the corresponding period. The riverine boundary conditions for DIN, DIP, DO, and SSC during summertime are listed in Table 1 for both the 1990s and 2010s cases. Notably, the 2010s SSC was set based on field data (Chen et al., 2020), whereas the 1990s SSC was back-calculated from the 2.5-fold difference in sediment loads. Long-term monitoring at river outlets showed no significant temporal trend in

chemical oxygen demand (COD) compared to the marked increases in nutrients and decreases in DO (Lai et al., 2022), indicating stable oxygen-consuming organic matters (OM) inputs. We therefore maintained constant OM concentrations between study periods (organic carbon: 2 mg/L; organic nitrogen: 0.2 mg/L; organic phosphorus: 0.03 mg/L), consistent with published historical observations (Wang et al., 2018). Furthermore, three additional model scenario simulations were conducted in order to disentangle the individual impact of each varying riverine input on the summer deoxygenation off the PRE. The setting of each scenario was identical to that of the 1990s case except that the riverine nutrients, SSC, and DO were separately replaced by the representative value in the 2010s (referring as to the "High-nutrient case", "Low-SSC case", and "DO-restore case", respectively; Table 1)

Table 1. Riverine inputs (in unit of mg L-1) for model experiments.

Cases	DIN	DIP	DO	SSC
1990s	1.0	0.020	6.5	100
2010s	2.0	0.065	3.5	40
High-nutrient	2.0	0.065	6.5	100
Low-SSC	1.0	0.020	6.5	40
DO-restore	2.0	0.065	6.5	40

# 3. Results

# 3.1 Responses of eutrophication to human-induced changes in

#### the PRE

## 3.1.1 Long-term variations in water quality distributions

To examine changes in eutrophication (a key process affecting DO dynamics) and its influential factors during summer in the PRE, we compared the simulated distributions of SSC, nutrients, Chl *a*, and POC in the surface waters between the 1990s and the 2010s cases (Fig. 3) as well as their vertical integrations in subregions (Table 2). Model results showed that the surface SSC within the PRE largely declined during

the two periods. In the 1990s, SSC maintained at a high level in the inner Lingdingyang Bay (see its location in Fig. 1b), ranging from 70.0 to 100.0 mg/L (Fig. 3a). Due to the particle sinking as waters advected downstream, SSC decreased to ~10.0 mg/L in the lower reaches of the PRE in the 1990s. While in the 2010s, the riverine sediment loads have remarkably decreased, resulting in a corresponding drawdown in SSC downstream (Fig. 3b-c). Overall, the vertically-integrated SSC content in the inner Lingdingyang Bay and lower PRE dropped by 56.1% and 45.6%-47.3% to 244.5 mg/m² and 38.4-69.2 mg/m², respectively (Table 2).

In terms of nutrients, the variation induced by riverine inputs was also evident during the two periods, acting on the main estuary in association with the spreading of the river plume. As shown, the DIN content in the 1990s was mostly below 1.5 mg/L within the entire PRE (Fig. 3d). With respect to the 2010s, the DIN concentration has increased by 0.8 mg/L and 0.2 mg/L in the surface waters of the upper Lingdingyang Bay and the lower PRE, respectively (Fig. 3e-f). The vertically-integrated DIN mass has increased by 41.9%-102% in the PRE (Table 2). A similar situation occurred with respect to DIP, with its content increasing from 0.04 mg/L in the 1990s to 0.07 mg/L in the 2010s in the high-DIP area adjacent to the middle Lingdingyang Bay (Fig. 3g-i). In terms of vertical integration, DIP increased by 9%-108%, with the lowest increases located in the Hong Kong waters downstream of the estuary (Table 2).

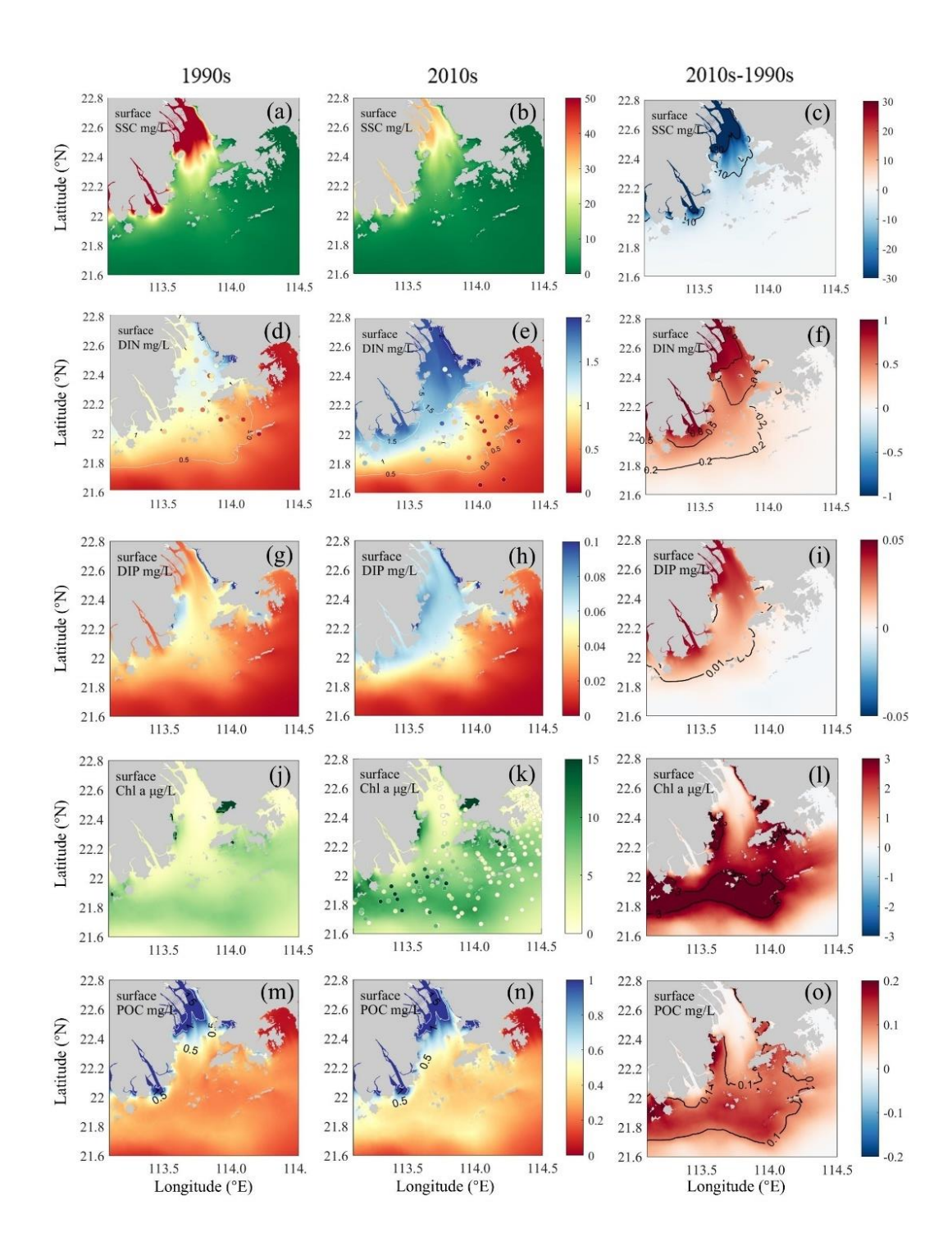


Fig. 3. Simulated surface water distributions in the PRE for (a-c) SSC, (d-f) DIN, (g-i) DIP, (j-l) Chl a, and (m-o) POC concentrations. Left panels (a, d, g, j, m) show 1990s conditions, middle panels (b, e, h, k, n) show 2010s conditions, and right panels (c, f, i, l, o) show their differences (2010s-1990s). Corresponding observations are indicated by colored dots in DIN (d, e) and Chl a (j, k) panels.

Table 2. Vertical integrations of DIN, DIP, SSC, Chl a, and POC contents; nutrient limitation index and euphotic depth; and DO concentrations, low-oxygen frequency (HF4), hypoxia frequency (HF3), and oxygen consumption rates in the bottom waters for subregions of the PRE (see locations in Fig. 1b) during the 1990s and the 2010s.

Carlono	Inner		Middle		Modaomen	ue ue	Outer			Const Const
Subregions	Lingdingyang Bay	ang Bay	Lingding	Lingdingyang Bay	sub-estuary	ry	Lingding	Lingdingyang Bay	nong no	nong wong waters
Cases	1990s	2010s	1990s	2010s	1990s	2010s	1990s	2010s	1990s	2010s
$DIN (mg m^{-2})$	6.58	12.24	5.42	9.20	4.89	7.62	5.17	7.92	3.62	5.14
$DIP (mg m^{-2})$	0.23	0.48	0.34	0.48	0.55	0.71	0.56	99.0	0.51	0.56
Nutrient limitation index 0.94	0.94	0.97	0.95	0.97	0.92	0.94	0.91	0.93	0.83	0.85
$SSC \text{ (mg m}^{-2}\text{)}$	556.5	244.5	332.9	164.6	120.4	63.4	127.7	69.2	9.07	38.4
Euphotic depth (m)	-1.3	-2.3	-2.0	-4.2	-9.5	-11.2	-11.8	-15.2	-20.7	-21.0
$\mathrm{Chl}\ a\ (\mu\mathrm{g}\ \mathrm{m}^{-2})$	5.0	7.1	11.7	22.9	39.4	70.4	40.7	72.9	74.3	108.9
$POC (mg m^{-2})$	9.8	8.64	8.8	5.31	4.82	6:39	5.33	6.85	6.21	7.91
Bottom DO (mg L <sup>-1</sup> )	4.55	3.52	4.31	3.90	3.50	2.84	4.96	4.12	4.36	3.52
HF4	25.0%	79.7%	26.8%	65.2%	84.5%	99.1%	4.5%	49.3%	20.5%	61.1%
HF3	6.5%	27.6%	4.8%	10.1%	25.2%	56.5%	3.5%	9.1%	4.8%	21.4%
$WCR~(mg~O_2~L^{-1}~day^{-1})$	-0.38	-0.45	-0.20	-0.25	-0.09	-0.11	-0.07	-0.09	-0.06	-0.07
$SOD (mg O_2 L^{-1} day^{-1})$	-1.72	-1.62	-0.89	-0.89	-0.24	-0.46	-0.28	-1.12	-0.91	-1.48

Note: HF4 (frequency of DO < 4 mg L<sup>-1</sup>); HF3 (frequency of DO < 3 mg L<sup>-1</sup>).

The euphotic depth is measured as negative values increasing downward from the sea surface.

In response to changes in light (affected by the SSC content) and nutrient conditions, phytoplankton biomass has substantially grown in the 2010s, indicated by the increased Chl a concentration. In the 1990s, the phytoplankton biomass was at a low level, with the Chl a generally below 8.0 µg/L in the surface waters (Fig. 3j). As for the 2010s, significant phytoplankton blooms were found along the Modaomen subestuary, outer Lingdingyang Bay, and Hong Kong waters (Fig. 3k-l), with the vertically-integrated Chl a content rising by 31.0 µg/m² (by 78.7% compared to the 1990s), 32.2 µg/m² (79.1%), and 34.6 µg/m² (46.6%), respectively (Table 2). As a result of the elevated primary production, a great amount of organic matter was produced in the PRE. Spatially coupled to the growth of Chl a (Fig. 3l), the POC content has significantly increased in the 2010s, especially in the lower PRE (Fig. 3m-o), with the vertically-integrated concentration increasing by 1.5-2.0 mg/m² (by 27.4%-32.6% compared to the 1990s) over the water column (Table 2).

## 3.1.2 Long-term variations in nutrient and light limitations

The primary production in the PRE was controlled by the synergistic effects of nutrient and light conditions. We calculate the nutrient limitation factor and the eutrophic depth to quantify the intensity of nutrient limitation and light limitation on algae growth. It should be noted that a smaller nutrient limitation index and a shallower eutrophic depth represent a stronger nutrient limitation and a stronger light limitation, respectively. Results showed that the nutrient limitation exhibited a distinct estuary-shelf gradient, in which the Hong Kong waters experienced more severe nutrient limitation than the Modaomen sub-estuary and Lingdingyang Bay (Fig. 4a, c). Specifically, the nutrient limitation index decreased from the upper estuary (0.94) to the Hong Kong waters (0.83) in the 1990s. In contrast, light limitation attenuated along the river plume transport pathway (Fig. 4b), largely ascribed to the decreasing SSC (Fig. 3a-b). Both observations and model simulations revealed consistent spatial patterns, with the eutrophic depth progressively increasing from severely light-limited regions near river outlets (Lingdingyang Bay: 1.3 m; Modaomen sub-estuary: 9.5 m) to the less-

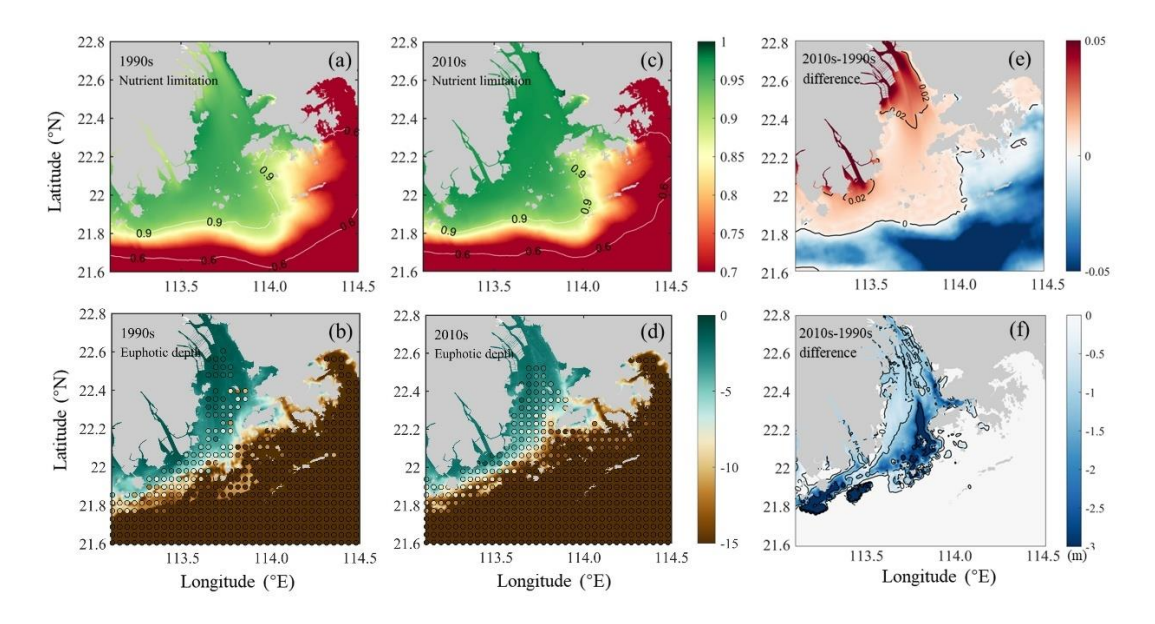


Fig. 4. Comparisons of (a, c) simulated nutrient limitation index for phytoplankton growth and (b, d) euphotic depths (in meters) between the 1990s and the 2010s, with their differences shown in (e) and (f), respectively. Colored dots in (b) and (d) represent corresponding euphotic depth observations. Note: Euphotic depth is measured as negative values increasing downward from the sea surface; thus, more negative differences in (f) indicate deeper light penetration in the 2010s.

The increased nutrient loads in the 2010s alleviated nutrient limitation. For instance, the nutrient limitation index in Hong Kong waters has increased to 0.85 (a 2.4% increase from the 1990s levels; Table 2). By contrast, the relief of light limitation due to the reduced riverine suspended sediments was more evident. Both model simulations and observations revealed significantly greater deepening of the euphotic depth in the Lingdingyang Bay compared to the lower estuary (Fig. 4b, d, f). In the inner Lingdingyang and middle Lingdingyang Bays, the euphotic depth increased by 1 m and 2.2 m (by 76.9% and 110.0% relative to the 1990s, Table2), respectively. The alterations in light conditions in the remaining area were relatively minor, with the eutrophic depth increasing to 11.2 m (by 17.9%) in the Modaomen sub-estuary and to 21 m (by 1.4%) in the Hong Kong waters during the 2010s (Table 2).

# 3.2 Responses of DO dynamics to human-induced changes in

# the PRE

# 3.2.1 Variations in DO distributions and hypoxia occurrences

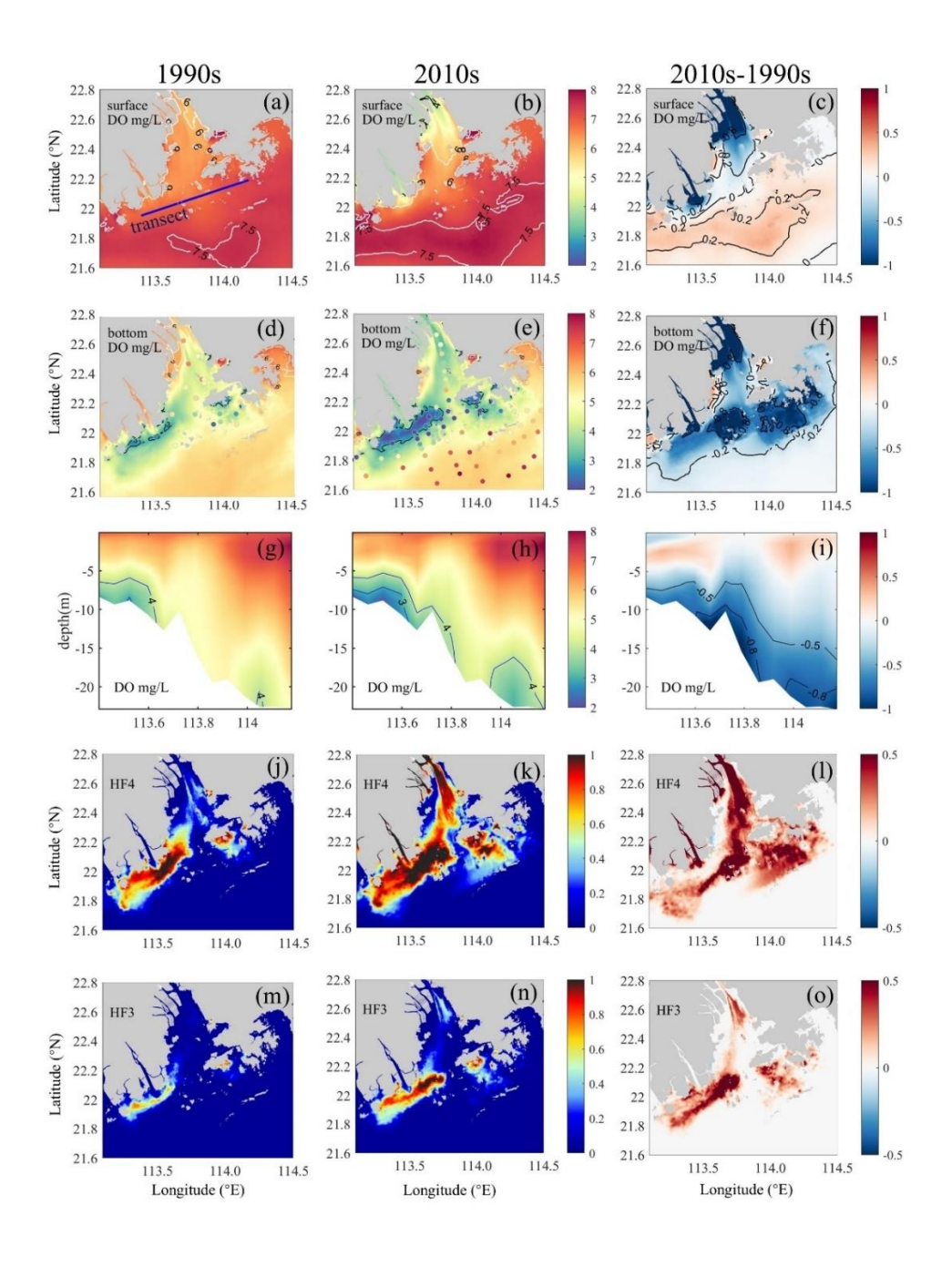


Fig. 5. (a-c) Surface DO and (d-f) bottom DO distributions, (g-i) vertical DO distributions along the transect (see its location in panel a), and (j-l) low-oxygen frequency (HF4, DO  $\leq$  4 mg/L) and (m-o) hypoxia frequency (HF3, DO  $\leq$  3 mg/L) in the bottom waters of the PRE for the 1990s (left panels) and the 2010s (middle panels)

as well as their differences (right panels). Note that hypoxia frequency is calculated as the number of hypoxic days divided by the total number of days in the study period, yielding a dimensionless ratio (range: 0–1).

Our model revealed distinct shifts in summertime DO patterns and hypoxia distribution (Fig. 5). The 1990s surface waters generally maintained DO >6 mg/L, increasing toward shelf regions (Fig. 5a). By the 2010s, surface DO increase by 0.2-0.3 mg/L (Fig. 5b-c), with an oxygen-enriched zone in the lower PRE correlating with high Chl a (Fig. 3k), though new low-oxygen zones (DO <4 mg/L) emerged near river outlets due to reduced Pearl River DO influx.

Bottom water simulations captured the hypoxia expansion from localized 1990s events (Fig. 2b-c) to widespread 2010s occurrences (Fig. 5d-e). Initial hypoxia clustered along the western PRE (Modaomen sub-estuary; Fig. 5d), with simulated HA4 (1179.7 km²) and HA3 (211.3 km²) (Table 3) matching observations (802±437 km² and 131±84 km²; 1994-1999 summers; Fig. 2a). By the 2010s, hypoxia intensified throughout Lingdingyang Bay and Hong Kong waters, with bottom DO declining to 2.8-4.1 mg/L (Table 2). Simulated HA4 expanded 1.5-fold to 2925.5 km² (Table 3), consistent with observed 2715±1068 km² (2013-2017; Fig. 2a). HA3 doubled to 617.2 km² by the 2010s, comparable to observed 901±591 km² (2013-2017).

Table 3. Simulated low-oxygen (HA4, DO < 4 mg/L) and hypoxic (HA3, DO < 3 mg/L) areas in the bottom waters of the PRE and their changes relative to the 1990s.

Cases	HA4 (km²)	Percentage of change	HA3 (km <sup>2</sup> )	Percentage of change
1990s	1179.7	/	211.3	/
2010s	2925.5	+148%	617.2	+192%
High-nutrient	1542.6	+31%	282.5	+34%
Low-SSC	1737.0	+47%	412.4	+95%
DO-restore	2409.7	+104%	617.2	+192%

Note: The calculation in percentage of change is:  $(HA_x-HA_{1990s})/HA_{1990s}$ , where x represents each case.

In addition, our model accurately reproduced the two observed hypoxic centers

along the coastal transition zone (Modaomen sub-estuary and Hong Kong waters; Fig. 2b-c), revealing distinct spatiotemporal deoxygenation patterns (Fig. 5g-o). During the 1990s, both centers exhibited limited low-oxygen zones, with Hong Kong waters showing <1 m thick DO <4 mg/L layers (Fig. 5g). Low-oxygen (HF4) and hypoxic

403 (HF3) conditions persisted 18-76 days (20.5%-84.5% frequency) and 4-23 days (4.8%-

25.2%) respectively during summer months (Fig. 5j, m; Table 2).

By the 2010s, hypoxic thickness increased substantially to ~1.5 m at Modaomen and ~5 m (~4 m thicker than 1990s) at Hong Kong waters (Fig. 5h). Event durations prolonged to 55-89 days (61.0%-99.1% HF4) and 19-51 days (21.4%-56.5% HF3) respectively (Fig. 5k, n; Table 2), demonstrating intensified and prolonged hypoxia.

# 3.2.2 Variations in bottom oxygen consumption

To further explore the mechanism of long-term deoxygenation off the PRE, we investigated the oxygen consumption rates and their changes during the two periods (the 1990s versus the 2010s). We specifically focused on the oxygen consumption at the bottom layers covering the 20% of the water depth above the sediments, where the majority of hypoxic events in the PRE occurred (Fig. 5).

As shown in Table 2, the predominant oxygen sink in the bottom waters of the PRE was sediment oxygen demand (SOD) induced largely by the remineralization of organic matter in sediments, whereas water column respiration (WCR) only accounted for 15.2% of the bottom oxygen consumption on average. Over the past three decades, both the WCR and SOD have generally increased in the PRE, primarily attributed to the growth in local production of organic matter associated with aggravated eutrophication (Fig. 3j-o). Particularly, the SOD in the outer Lingdingyang Bay and Hong Kong waters has remarkably increased from 0.28-0.92 mg O<sub>2</sub> L<sup>-1</sup> day<sup>-1</sup> in the 1990s to 1.12-1.48 mg O<sub>2</sub> L<sup>-1</sup> day<sup>-1</sup> in the 2010s (Table 2), which contributed to 80%~95% of the increment in total oxygen consumption. Although the absolute increase of SOD in the Modaomen sub-estuary was comparatively small, the SOD in the 2010s has almost doubled compared to the 1990s, leading to a substantial increase in the

occurrence of hypoxic events in this region (Fig. 5d-o).

428

429

430

431

432

433

434

435

436

437

438

439

440

441

442

443

444

445

446

447

448

449

450

451

452

# 3.2.3 Disentangling contributions of riverine oxygen, suspended sediments, and nutrient changes on deoxygenation

As detailed in Section 2.3, three scenario simulations were performed to quantify the relative contributions of riverine changes to the decadal low-oxygen expansion in the PRE (Table 1). In general, the riverine impacts on DO and related biogeochemical factors varied significantly between subregions (Figs. 6-7). Specifically, increasing the riverine nutrient levels from the 1990s to the 2010s alone (High-nutrient case) led to a marked drawdown in the bottom DO around the lower PRE (by over 0.2 mg/L relative to the 1990s; Fig. 6a). The DO decline, extending from the Modaomen sub-estuary to the Hong Kong waters, was ascribed to the elevated phytoplankton biomass (Fig. 7b) facilitated by better nutrient conditions, which subsequently sustained stronger bottom oxygen depletions compared to the 1990s (Fig. 7c). Among the subregions, the Hong Kong waters was more susceptible to the changes in riverine nutrients as it was subject to comparatively severe nutrient limitation (Table 2). Therefore, with the improvement of nutrient utilization, this region experienced more pronounced deoxygenation in association with significant alterations in Chl a content and SOD (increased by 14.2 μg/m<sup>2</sup> and 0.26 mg O<sub>2</sub> L<sup>-1</sup> day<sup>-1</sup>, respectively, equivalent to 47.1% and 46.4% of their total increments over the past three decades; Fig. 7). While in the inner Lingdingyang Bay, the increased nutrient inputs only caused a slight change in Chl a content because the phytoplankton growth in this region was mostly light limited due to high water turbidity (Table 2). The concomitant changes in SOD and bottom DO were fairly small as well. Collectively, the high-nutrient scenario alone resulted in a 31% and 34% growth in the area affected by low oxygen (HA4) and hypoxia (HA3) relative to the 1990s, respectively (Table 3).

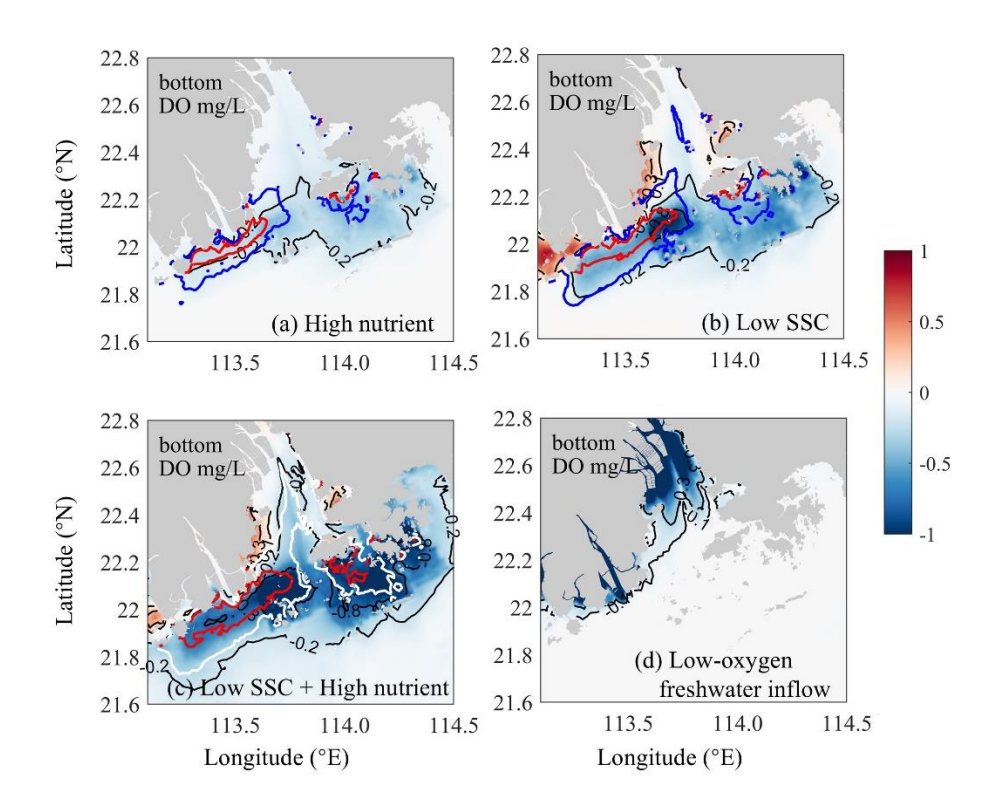


Fig. 6. Bottom DO changes induced by (a) riverine nutrient increases (the High-nutrient case minus the 1990s case), (b) riverine SSC declines (the Low-SSC case minus the 1990s case), (c) the combined effects of nutrient increases and SSC declines (the DO-restore case minus the 1990s case), and (d) riverine DO declines (the DO-restore case minus the 2010s case), respectively. The blue and white contour lines represent DO = 4 mg/L for the respective cases, and the red contour lines represent DO = 3 mg/L.

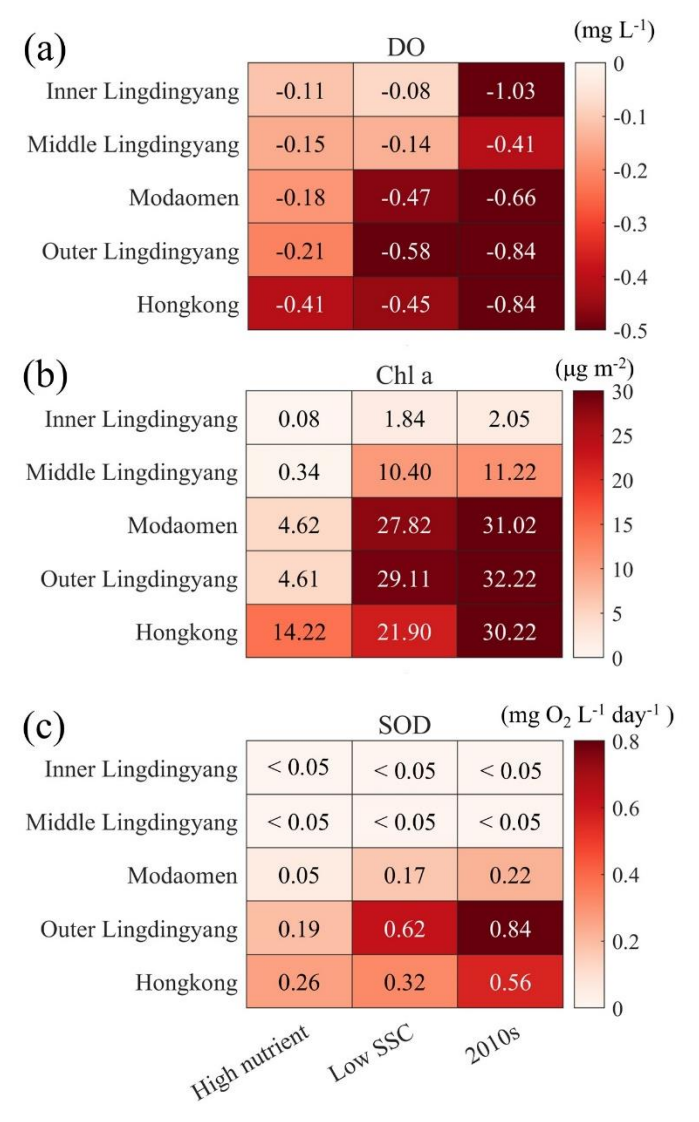


Fig. 7. Changes of (a) bottom DO concentration, (b) vertically-integrated Chl a content, and (c) SOD in subregions of the PRE for the High-nutrient, the Low-SSC, and the 2010s cases relative to the 1990s case.

Compared with the High-nutrient case, reducing the riverine suspended sediment loads from the 1990s to the 2010s alone (Low-SSC case) imposed a greater impact on the DO conditions, causing more extensive and intense deoxygenation through the PRE (Fig. 6b). Apparent DO decline (exceeding 0.3 mg/L relative to the 1990s) occurred within the lower PRE, similar to that of the changing riverine nutrients described above. This is also attributed to the intensified SOD (with an increment of 0.17-0.62 mg O<sub>2</sub> L<sup>-1</sup> day<sup>-1</sup>, accounting for 57.1%-77.3% of the total increment during the two periods; Fig.

7c), accompanied by a prominent increase in Chl a content (by  $21.9-29.1 \text{ µg/m}^2$ , accounting for 72.4%-90.3% of the total increment; Fig. 7b) due to the improved light condition (the relief of light limitation; Table 2). The SSC-induced changes in these biogeochemical factors were more pronounced in the outer Lingdingyang Bay and Modaomen sub-estuary than in other regions including the Hong Kong waters, which coincided with the alterations in deoxygenation among the subregions (Fig. 7). Overall, under the low-SSC scenario the low-oxygen area (HA4) and hypoxic area (HA3) expanded by 47% and 95% compared to the 1990s, respectively (Table 3). As shown in Figure 7 and Table 3, the combined effect of reducing SSC and increasing nutrient inputs (DO-restore case) led to a significant expansion of low-oxygen conditions, with hypoxic areas (HA4) and low-oxygen areas (HA3) reaching 2409.7 km<sup>2</sup> and 617.2 km<sup>2</sup>, respectively. This combined effect exceeded the sum of changes induced by individual river inputs, highlighting the non-linear interaction between SSC and nutrient loading. In regions such as Outer Lingdingyang and Hong Kong, the combined effect was amplified, while in regions such as Inner and Middle Lingdingyang, the combined effect was less than the sum of individual effects. The growth of phytoplankton is not a linear process in response to various influencing factors; instead, these factors interact cumulatively. Therefore, when different factors are combined, their combined effect can exceed the impact of individual factors acting alone.

473

474

475

476

477

478

479

480

481

482

483

484

485

486

487

488

489

490

491

492

493

494

495

496

497

498

499

500

With respect to the influence of altered riverine DO influx, it could be deduced from the difference between the 2010s and the DO-restore cases (Fig. 6d). There was a considerable DO decrease (by over 0.8 mg/L) in the bottom waters adjacent to the river outlets (also in the surface waters) owing to the low-oxygen inflows from the upstream river channels. The impact of these low-oxygen waters was largely restricted within the upper Lingdingyang Bay under the effects of air-sea reoxygenation and water-column mixing along with the river plume transport. Collectively, reducing the riverine DO content from the 1990s to the 2010s alone resulted in an enlargement of low-oxygen area by nearly 515.8 km² (derived by subtracting the HA4 of the 2010s case from that

of the DO-restore case; Table 3).

#### 4. Discussion

501

502

503

504

505

506

507

508

509

510

511

512

513

514

515

516

517

518

519

520

521

522

523

524

525

526

# 4.1 Impacts of decadal changes in riverine inputs on

By integrating long-term observations with physical-biogeochemical model

## deoxygenation off the PRE

simulations, we revealed significant bottom-water deoxygenation in the Pearl River Estuary over the past three decades, driven by changes in riverine inputs. From the 1990s to 2010s, summer inflows of DIN and DIP increased by ~100% and ~225%, while SSC decreased by ~60% due to human activities like dam construction (Liu et al., 2022) and reforestation (Cao et al., 2023). Concurrently, oxygen depletion from terrestrial pollutants reduced riverine DO concentrations by 46% (Ma et al., 2024). These shifts collectively intensified bottom-water low-oxygen conditions in PRE (Fig. 5), with model simulations showing a 148% expansion in summer low-oxygen areas (DO < 4 mg/L) and a 192% increase in hypoxic areas (DO < 3 mg/L). Low-oxygen events also become more persistent, lasting longer (~15-35 days during June-August) and expanding vertically by  $\sim$ 1-4 m (Fig 5.g-h). More interestingly, the PRE has developed three distinct hypoxic centers (including the inner Lingdingyang Bay, Modaomen sub-estuary, and Hong Kong waters) controlled by different dominant factors, which renders the deoxygenation problem in this region as a great reference for estuaries and coastal systems worldwide. Specifically, the impact of riverine low-oxygen waters was confined within the upper estuary close to the river outlets, leading to a ~44% increase in the low-oxygen area relative to the 1990s. Such local low-oxygen issue could be mitigated to a large extent if the riverine DO recovered to a comparatively higher level (e.g., ~6.5 mg/L in the 1990s) according to the DO-restore scenario (Fig. 6d). Reduced water turbidity downstream facilitates the upstream transport of nutrients, promoting eutrophication and oxygen depletion in

the lower reaches, which is highly sensitive to changes in riverine nutrient and sediment inputs. As indicated in the High-nutrient and the Low-SSC cases, the increased nutrient inputs and declined suspended sediment loads have separately alleviated the nutrient and light limitations on algae growth in the region, thereby stimulating phytoplankton blooms and local production of organic matter to support subsurface oxygen consumption (dominated by sediment oxygen uptake, SOD; Fig. 7).

While previous studies have primarily examined the impacts of riverine inputs of freshwater, nutrients and organic matter, this study provides a comprehensive investigation of how suspended sediment reduction influences estuarine dissolved oxygen dynamics. In the PRE, the riverine SSC reduction played a more important role in driving the long-term low-oxygen expansion than nutrient increase. Its synergistic effect with the riverine nutrient changes could further amplify the exacerbation of eutrophication and subsequent deoxygenation, resulting in an enlarged growth in the low-oxygen area (by 104%) and hypoxic area (by 192%) that was notably larger than the total of their partial contributions (Table 3), and reached 70% of the total impact from combined SSC, nutrient, and low-oxygen changes (148% low-oxygen expansion).

It is worth mentioning that the relative importance of the riverine nutrient and SSC changes were different between the two hypoxic centers in the lower PRE, depending upon their distances and water flow conditions from the river outlets. Closer to the river outlets, the Modaomen sub-estuary and its surrounding waters (located on the western side of the coastal transition zone off the PRE) possessed a fairly high SSC level, which imposed a stronger light limitation on the growth of phytoplankton in the region, ultimately making the oxygen dynamics more susceptible to the decline in riverine SSC. This non-additive characteristic underscores the need for integrated management approaches that simultaneously address both nutrient loads and suspended sediment-mediated light conditions.

Suspended sediments were confined to the coastal area of Modaomen by water currents (Fig. 1b), resulting in a significant decrease in sediment deposition in this

region, which greatly improved light availability, ultimately making the oxygen dynamics more susceptible to the decline in riverine SSC. On the contrary, the Hong Kong waters and adjacent coastal areas (located on the eastern side of the coastal transition zone) far from the river outlets were less affected by the riverine inputs, where the relatively low nutrient levels promoted more sensitive responses of biogeochemical processes (e.g. primary production and SOD) and hypoxia occurrences to nutrient variations. Besides, the complex island topography near Hong Kong (Fig. 1b) creates hydrodynamic barriers that restrict the offshore transport of suspended sediments.

# 4.2 Nutrient control and hypoxia mitigation in the context of

# sediment declines

Our results highlight the substantial spatial variability in how riverine inputs influence deoxygenation, emphasizing the need for more targeted strategies to mitigate hypoxia. While the effects of riverine nutrients on hypoxia have been widely studied, the role of SSC in modulating eutrophication and hypoxia has received comparatively less attention. This is particularly relevant in systems like the PRE, which has experienced a dramatic 60% decline in sediment since the 1980s due to dam construction and land-use changes.

In the PRE, our model simulations demonstrate that SSC-mediated light limitation critically influences deoxygenation dynamics. When SSC declines are omitted, model simulations overestimate nutrient-driven productivity and underestimate hypoxia expansion. This suggests that for systems experiencing pronounced sediment reductions, overlooking SSC effects could lead to overly optimistic assessments of nutrient control efficacy. It is therefore critical to disentangle the relative contributions of riverine nutrients versus SSC changes to coastal deoxygenation trend. As demonstrated in the PRE, the current low-SSC environment suggests that more stringent nutrient reductions might be required to effectively curb deoxygenation compared to conditions with higher SSC.

Although dam constructions in the Pearl River Basin, mostly completed before the 2000s, have driven significant declines in SSC, the future trends of riverine SSC remain uncertain. For instance, recent reforestation efforts have effectively reduced summer freshwater discharge and sediment load in the Pearl River Basin (Cao et al., 2023). This evolving situation underscores that changes in SSC will continue to shape future oxygen dynamics, introducing compounding uncertainties for hypoxia mitigation.

Similar relationship between SSC and eutrophication or hypoxia have been observed in other systems facing rapid anthropogenic changes. For example, the Yangtze River Estuary has seen a ~56% decrease in SSC over the past decades, which has been linked to a 61% increase in Chl *a* concentration, indicating intensified eutrophication (Wang et al., 2019). In addition, several modelling studies have shown that dam constructions in the upper regions of the Guadiana Estuary have led to reduced water turbidity and exacerbated eutrophication in the lower estuary (Domingues et al., 2012; Barbosa et al., 2010). A global survey revealed that sediment loads in 414 major rivers have decreased by approximately 51% since the 2000s due to human activities (Dethier et al., 2022). This trend highlights the need for further investigation into how sediment declines impact eutrophication and deoxygenation on a global scale.

It is also important to recognize that human activities can increase sediment loads in estuaries. For example, land-use changes such as deforestation\_(Kasai et al., 2005) and industrialization (Syvitski and Kettner, 2011) can exacerbate soil erosion and sediment transport, leading to higher suspended sediment concentrations in the water. In such cases, light attenuation due to increased turbidity may suppress phytoplankton growth and reduce primary production, potentially mitigating hypoxia. Therefore, the effects of SSC are system-specific and depend on the direction and magnitude of sediment trends.

Some caveats in our work require further investigation. First, our light attenuation parameterization is based on the empirical formulation of Ditoro (2001), which has been validated for the PRE through biogeochemical consistency checks (Wang et al.,

2018). While this approach successfully captured observed oxygen dynamics in our simulations, it explicitly resolves only the chlorophyll and suspended sediment effects on light attenuation. Previous studies have shown that colored dissolved organic matter (CDOM) also plays a significant role in light attenuation within the PRE (Cao et al., 2003; Wang et al., 2010), particularly during algal bloom periods. The model's calibration to observed biogeochemical variables may partially compensate for CDOM's influence, but future work should explicitly parameterize CDOM's optical properties through both modeling refinements and sustained monitoring to better quantify its role in oxygen dynamics. In addition to anthropogenic influences, changes in regional physical conditions due to climate change, such as wind speed and freshwater discharge, could also affect the long-term deoxygenation trends in coastal regions (Yu et al., 2015; Chen et al., 2024). The impacts of ocean warming on deoxygenation (Laurent et al., 2018) remain unclear in the PRE despite evidence of warming (Cheung et al., 2021). The compounding factors of warming such as sea-level rise (Hong et al., 2020) may introduce further complexity to hypoxia dynamics through cascading ecosystem effects. While these factors were not considered in this study, understanding the interplay between human activities and climate changes is crucial for future research on oxygen dynamics and hypoxia development in estuaries and coastal systems.

# 5. Conclusion

610

611

612

613

614

615

616

617

618

619

620

621

622

623

624

625

626

627

628

629

630

631

632

633

634

635

636

We applied a well-validated physical-biogeochemical model to reconstruct the summertime oxygen distributions in the PRE during two representative periods (the 1990s and the 2010s) and to disentangle the contribution of alterations in riverine inputs (i.e., suspended sediments, nutrients, and oxygen concentration) to the long-term deoxygenation off the PRE based on a suite of model experiments. We found that owing to the changes of riverine inputs over the past three decades, the low-oxygen and hypoxic areas in the bottom waters of the PRE have expanded by about 1.5 times and

two-fold, respectively, with the duration time prolonged by ~15-35 days in summer. Concurrently, three hypoxic centers dominated by distinct factors were identified. Single-factor experiments suggested that a 46% decrease in riverine DO alone expanded low-oxygen areas by ~44% in the upper PRE, a 60% SSC reduction alone caused a 47% expansion in the lower PRE, and nutrient increases alone (100% DIN, 225% phosphate) drove a 31% expansion. By comparison, the alterations in riverine nutrients and suspended sediments have separately provided better nutrient and light conditions to promote higher production of labile organic matter, which jointly maintained considerable oxygen depletions and exacerbated the low-oxygen conditions in the lower PRE. The relative importance of the changing riverine nutrients and suspended sediments to deoxygenation varied between subregions. The suspended sediment reduction was the predominated factor in the downstream regions close to the river outlets (e.g. the Modaomen sub-estuary), while the nutrient increase exerted a more substantial influence in the regions far from the river outlets (e.g. the Hong Kong waters). Our study demonstrates that declined suspended sediments have significantly exacerbated low-oxygen conditions off the PRE, with effects that synergistically intensify when combined with increasing nutrient loads. These findings highlight the need for dual-control strategies addressing both nutrient inputs and sediment-mediated light availability in coastal management. Give the global declines in riverine suspended sediments, we emphasize that effective hypoxia mitigation requires integrated approaches accounting for these interacting drivers.

658

659

660

661

662

663

637

638

639

640

641

642

643

644

645

646

647

648

649

650

651

652

653

654

655

656

657

# **CRediT** authorship contribution statement

YN: Investigation, Model experiments, Formal analysis, Visualization, Writing-original draft. ZC: Model experiments, Writing-review. BW: Writing-review. BL: Writing-review. JH: Project administration, Supervision, Conceptualization, Writing-review & editing.

#### **Declaration of competing interest**

The authors declare that they have no known competing financial interests or personal relationships that could have appeared to influence the work reported in this paper.

#### Acknowledgements

664

668

674

685

This work was supported by the National Natural Science Foundation of Guangdong Province (grant no. 2025A1515010991) and a grant from the Southern Marine Science and Engineering Guangdong Laboratory (Zhuhai) (Project. SML2024SP024) to JH, and the National Natural Science Foundation of China (grand no. 42206141) to LB.

## Data availability

The dissolved oxygen observation datasets off the Pearl River Estuary were 675 obtained from published studies (Hu et al., 2021, DOI: 10.5194/bg-18-5247-2021; Su 676 677 DOI: 10.5194/bg-14-4085-2017; Li et al., 2021. DOI: 10.1029/2020JC016700; Chen et al., 2020, DOI: 10.1029/2019JG005596) and the 678 679 Environmental Hong Kong Protection Department 680 (https://cd.epic.epd.gov.hk/EPICRIVER/marine/). The observed nutrients, oxygen, and 681 suspended sediments data in the Pearl River are available from Hu et al. (2021) and 682 publicly accessible databases maintained by Department of Ecology and Environment of Guangdong Province (https://gdee.gd.gov.cn/hjjce/jahy/index.html) and the China 683 684 River Sediment Bulletin (http://www.mwr.gov.cn/sj/tjgb/zghlnsgb/).

#### 686 Reference

- Barbosa, A. B., Domingues, R. B., and Galvão, H. M.: Environmental Forcing of
- 688 Phytoplankton in a Mediterranean Estuary (Guadiana Estuary, South-western Iberia):
- A Decadal Study of Anthropogenic and Climatic Influences, Estuaries and Coasts, 33,
- 690 324-341, https://doi.org/10.1007/s12237-009-9200-x, 2010.
- 691 Bianchi, T. S., DiMarco, S. F., Cowan, J. H., Hetland, R. D., Chapman, P., Day, J. W.,
- and Allison, M. A.: The science of hypoxia in the Northern Gulf of Mexico: A review,
- 693 Science of The Total Environment, 408, 1471-1484,
- 694 https://doi.org/10.1016/j.scitotenv.2009.11.047, 2010.
- 695 Breitburg, D., Levin, L. A., Oschlies, A., Grégoire, M., Chavez, F. P., Conley, D. J.,
- 696 Garçon, V., Gilbert, D., Gutiérrez, D., Isensee, K., Jacinto, G. S., Limburg, K. E.,
- Montes, I., Naqvi, S. W. A., Pitcher, G. C., Rabalais, N. N., Roman, M. R., Rose, K. A.,
- 698 Seibel, B. A., Telszewski, M., Yasuhara, M., and Zhang, J.: Declining oxygen in the
- 699 global ocean and coastal waters, Science, 359, eaam7240,
- 700 https://doi.org/10.1126/science.aam7240, 2018.
- 701 Bussi, G., Darby, S. E., Whitehead, P. G., Jin, L., Dadson, S. J., Voepel, H. E.,
- Vasilopoulos, G., Hackney, C. R., Hutton, C., Berchoux, T., Parsons, D. R., and
- Nicholas, A.: Impact of dams and climate change on suspended sediment flux to the
- 704 Mekong delta, Science of The Total Environment, 755, 142468,
- 705 https://doi.org/10.1016/j.scitotenv.2020.142468, 2021.
- Cao, W., Yang, Y., Xu, X., Huang, L., and Zhang, J.: Regional patterns of particulate
- spectral absorption in the Pearl River estuary, Chinese Science Bulletin, 48, 2344-2351,
- 708 https://doi.org/10.1360/03wd0151, 2003.
- 709 Cao, Z., Duan, H., Ma, R., Shen, M., and Yang, H.: Remarkable effects of greening
- 710 watershed on reducing suspended sediment flux in China's major rivers, Science
- 711 Bulletin, 68, 2285-2288, https://doi.org/10.1016/j.scib.2023.08.036, 2023.
- Carstensen, J., Andersen, J. H., Gustafsson, B. G., and Conley, D. J.: Deoxygenation of
- 713 the Baltic Sea during the last century, Proceedings of the National Academy of Sciences
- 714 of the United States of America, 111, 5628-5633,
- 715 https://doi.org/10.1073/pnas.1323156111, 2014.
- 716 Chen, J. Y., Pan, D. L., Liu, M. L., Mao, Z. H., Zhu, O. K., Chen, N. H., Zhang, X. Y.,
- 717 and Tao, B. Y.: Relationships Between Long-Term Trend of Satellite-Derived
- 718 Chlorophyll-a and Hypoxia Off the Changjiang Estuary, ESTUARIES AND COASTS,
- 719 40, 1055-1065, https://doi.org/10.1007/s12237-016-0203-0, 2017.
- 720 Chen, L., Zhang, X., He, B., Liu, J., Lu, Y., Liu, H., Dai, M., Gan, J., and Kao, S.-J.:
- 721 Dark Ammonium Transformations in the Pearl River Estuary During Summer, Journal
- 722 of Geophysical Research: Biogeosciences, 125, e2019JG005596,
- 723 https://doi.org/10.1029/2019JG005596, 2020.
- 724 Chen, Z., Yu, L., and Hu, J.: Disentangling the contributions of anthropogenic nutrient
- 725 input and physical forcing to long-term deoxygenation off the Pearl River Estuary,
- 726 China, Water Research, 265, 122258, https://doi.org/10.1016/j.watres.2024.122258,

- 727 2024.
- 728 Cheung, Y. Y., Cheung, S., Mak, J., Liu, K., Xia, X., Zhang, X., Yung, Y., and Liu, H.:
- 729 Distinct interaction effects of warming and anthropogenic input on diatoms and
- dinoflagellates in an urbanized estuarine ecosystem, Global Change Biology, 27, 3463-
- 731 3473, https://doi.org/10.1111/gcb.15667, 2021.
- Cormier, J. M., Coffin, M. R. S., Pater, C. C., Knysh, K. M., Gilmour, R. F., Guyondet,
- 733 T., Courtenay, S. C., and van den Heuvel, M. R.: Internal nutrients dominate load and
- drive hypoxia in a eutrophic estuary, Environmental Monitoring and Assessment, 195,
- 735 1211, https://doi.org/10.1007/s10661-023-11621-y, 2023.
- 736 Cullen, J. J.: Subsurface Chlorophyll Maximum Layers: Enduring Enigma or Mystery
- 737 Solved?, in: ANNUAL REVIEW OF MARINE SCIENCE, VOL 7, edited by: Carlson,
- 738 C. A., and Giovannoni, S. J., 207-239, 10.1146/annurev-marine-010213-135111, 2015.
- 739 Dethier, E. N., Renshaw, C. E., and Magilligan, F. J.: Rapid changes to global river
- 740 suspended sediment flux by humans, Science, 376, 1447-1452,
- 741 https://doi.org/10.1126/science.abn7980, 2022.
- 742 Diaz, R. J. and Rosenberg, R.: Spreading dead zones and consequences for marine
- 743 ecosystems, Science, 321, 926-929, https://doi.org/10.1126/science.1156401, 2008.
- 744 DiToro, D. M.: Sediment flux modeling, John Wiley & Sons, 656 pp., ISBN
- 745 9780471135357, 2001.
- 746 Domingues, R. B., Barbosa, A. B., Sommer, U., and Galvão, H. M.: Phytoplankton
- composition, growth and production in the Guadiana estuary (SW Iberia): Unraveling
- changes induced after dam construction, Science of The Total Environment, 416, 300-
- 749 313, https://doi.org/10.1016/j.scitotenv.2011.11.043, 2012.
- 750 Ge, J., Torres, R., Chen, C., Liu, J., Xu, Y., Bellerby, R., Shen, F., Bruggeman, J., and
- 751 Ding, P.: Influence of suspended sediment front on nutrients and phytoplankton
- dynamics off the Changjiang Estuary: A FVCOM-ERSEM coupled model experiment,
- 753 Journal of Marine Systems, 204, 103292,
- 754 https://doi.org/10.1016/j.jmarsys.2019.103292, 2020.
- Hagy, J. D., Boynton, W. R., and Jasinski, D. A.: Modelling phytoplankton deposition
- 756 to Chesapeake Bay sediments during winter-spring: interannual variability in relation
- 757 to river flow, ESTUARINE COASTAL AND SHELF SCIENCE, 62, 25-40,
- 758 https://doi.org/10.1016/j.ecss.2004.08.004, 2005.
- Hong, B., Liu, Z., Shen, J., Wu, H., Gong, W., Xu, H., and Wang, D.: Potential physical
- 760 impacts of sea-level rise on the Pearl River Estuary, China, Journal of Marine Systems,
- 761 201, 103245, https://doi.org/10.1016/j.jmarsys.2019.103245, 2020.
- Howarth, R., Chan, F., Conley, D. J., Garnier, J., Doney, S. C., Marino, R., and Billen,
- 763 G.: Coupled biogeochemical cycles: eutrophication and hypoxia in temperate estuaries
- and coastal marine ecosystems, Frontiers in Ecology and the Environment, 9, 18-26,
- 765 https://doi.org/10.1890/100008, 2011.
- Hu, J. and Li, S.: Modeling the mass fluxes and transformations of nutrients in the Pearl
- 767 River Delta, China, Journal of Marine Systems, 78, 146-167,
- 768 https://doi.org/10.1016/j.jmarsys.2009.05.001, 2009.

- Hu, J., Li, S., and Geng, B.: Modeling the mass flux budgets of water and suspended
- sediments for the river network and estuary in the Pearl River Delta, China, Journal of
- 771 Marine Systems, 88, 252-266, https://doi.org/10.1016/j.jmarsys.2011.05.002, 2011.
- Hu, J., Zhang, Z., Wang, B., and Huang, J.: Long-term spatiotemporal variations in and
- expansion of low-oxygen conditions in the Pearl River estuary: a study synthesizing
- 774 observations during 1976–2017, Biogeosciences, 18, 5247-5264,
- 775 https://doi.org/10.5194/bg-18-5247-2021, 2021.
- 776 Huang, Y.-G., Yang, H.-F., Jia, J.-J., Li, P., Zhang, W.-X., Wang, Y. P., Ding, Y.-F., Dai,
- 777 Z.-J., Shi, B.-W., and Yang, S.-L.: Declines in suspended sediment concentration and
- 778 their geomorphological and biological impacts in the Yangtze River Estuary and
- 779 adjacent sea, Estuarine, Coastal and Shelf Science, 265, 107708,
- 780 https://doi.org/10.1016/j.ecss.2021.107708, 2022.
- HydroQual, Inc.: User's Guide for RCA (Release 3.0), HydroQual, Inc., Mahwah, NJ,
- 782 2004.
- 783 Kasai, M., Brierley, G. J., Page, M. J., Marutani, T., and Trustrum, N. A.: Impacts of
- land use change on patterns of sediment flux in Weraamaia catchment, New Zealand,
- 785 CATENA, 64, 27-60, https://doi.org/10.1016/j.catena.2005.06.014, 2005.
- Lai, Y., Jia, Z., Xie, Z., Li, S., and Hu, J.: Water quality changes and shift in mechanisms
- 787 controlling hypoxia in response to pollutant load reductions: A case study for Shiziyang
- 788 Bay, Southern China, Science of The Total Environment, 842, 156774,
- 789 https://doi.org/10.1016/j.scitotenv.2022.156774, 2022.
- 790 Laurent, A., Fennel, K., Ko, D. S., and Lehrter, J.: Climate change projected to
- 791 exacerbate impacts of coastal eutrophication in the northern Gulf of Mexico, Journal of
- 792 Geophysical Research: Oceans, 123, 3408-3426,
- 793 https://doi.org/10.1002/2017JC013583, 2018.
- Lee, Z.-P., Du, K.-P., and Arnone, R.: A model for the diffuse attenuation coefficient of
- 795 downwelling irradiance, Journal of Geophysical Research: Oceans, 110,
- 796 https://doi.org/10.1029/2004JC002275, 2005.
- 797 Li, D., Gan, J., Hui, C., Yu, L., Liu, Z., Lu, Z., Kao, S.-j., and Dai, M.: Spatiotemporal
- 798 Development and Dissipation of Hypoxia Induced by Variable Wind-Driven Shelf
- 799 Circulation off the Pearl River Estuary: Observational and Modeling Studies, Journal
- 800 of Geophysical Research: Oceans, 126, e2020JC016700,
- 801 https://doi.org/10.1029/2020JC016700, 2021.
- 802 Li, G., Liu, J., Diao, Z., Jiang, X., Li, J., Ke, Z., Shen, P., Ren, L., Huang, L., and Tan,
- Y:: Subsurface low dissolved oxygen occurred at fresh- and saline-water intersection of
- the Pearl River estuary during the summer period, Marine Pollution Bulletin, 126, 585-
- 805 591, https://doi.org/10.1016/j.marpolbul.2017.09.061, 2018.
- 806 Li, X., Lu, C., Zhang, Y., Zhao, H., Wang, J., Liu, H., and Yin, K.: Low dissolved
- 807 oxygen in the Pearl River estuary in summer: Long-term spatio-temporal patterns,
- 808 trends, and regulating factors, Marine Pollution Bulletin, 151, 110814,
- 809 https://doi.org/10.1016/j.marpolbul.2019.110814, 2020.
- 810 Liu, Z., Fagherazzi, S., Liu, X., Shao, D., Miao, C., Cai, Y., Hou, C., Liu, Y., Li, X., and

- 811 Cui, B.: Long-term variations in water discharge and sediment load of the Pearl River
- 812 Estuary: Implications for sustainable development of the Greater Bay Area, Frontiers
- 813 in Marine Science, 9, 983517, https://doi.org/10.3389/fmars.2022.983517, 2022.
- 814 Lu, Z., Gan, J., Dai, M., Liu, H., and Zhao, X.: Joint Effects of Extrinsic Biophysical
- 815 Fluxes and Intrinsic Hydrodynamics on the Formation of Hypoxia West off the Pearl
- 816 River Estuary, Journal of Geophysical Research: Oceans, 123, 6241-6259,
- 817 https://doi.org/10.1029/2018jc014199, 2018.
- 818 Luo, X., Yang, Q., and Jia, L.: The Riverbed Evolution of the River-Network System
- in the Pearl River Delta, Sun Yat-sen University Press, Guangzhou, China, 2002.
- 820 Ma, C., Zhao, J., Ai, B., Sun, S., and Yang, Z.: Machine Learning Based Long-Term
- Water Quality in the Turbid Pearl River Estuary, China, Journal of Geophysical
- 822 Research: Oceans, 127, e2021JC018017, https://doi.org/10.1029/2021JC018017, 2022.
- Ma, R., Chen, Z., Wang, B., Xu, C., Jia, Z., Li, L., and Hu, J.: Spatiotemporal variations
- and controlling mechanism of low dissolved oxygen in a highly urbanized complex
- 825 river system, Journal of Hydrology: Regional Studies, 52, 101691,
- 826 https://doi.org/10.1016/j.ejrh.2024.101691, 2024.
- 827 Murphy, R. R., Kemp, W. M., and Ball, W. P.: Long-Term Trends in Chesapeake Bay
- 828 Seasonal Hypoxia, Stratification, and Nutrient Loading, ESTUARIES AND COASTS,
- 829 34, 1293-1309, https://doi.org/10.1007/s12237-011-9413-7, 2011.
- Pitcher, G. C., Aguirre-Velarde, A., Breitburg, D., Cardich, J., Carstensen, J., Conley,
- 831 D. J., Dewitte, B., Engel, A., Espinoza-Morriberón, D., Flores, G., Garçon, V., Graco,
- 832 M., Grégoire, M., Gutiérrez, D., Hernandez-Ayon, J. M., Huang, H.-H. M., Isensee, K.,
- Jacinto, M. E., Levin, L., Lorenzo, A., Machu, E., Merma, L., Montes, I., Swa, N.,
- Paulmier, A., Roman, M., Rose, K., Hood, R., Rabalais, N. N., Salvanes, A. G. V.,
- 835 Salvatteci, R., Sánchez, S., Sifeddine, A., Tall, A. W., Plas, A. K. v. d., Yasuhara, M.,
- 836 Zhang, J., and Zhu, Z. Y.: System controls of coastal and open ocean oxygen depletion,
- 837 Progress in Oceanography, 197, 102613, https://doi.org/10.1016/j.pocean.2021.102613,
- 838 2021.
- Roman, M. R., Brandt, S. B., Houde, E. D., and Pierson, J. J.: Interactive effects of
- 840 Hypoxia and temperature on coastal pelagic zooplankton and fish, Frontiers in Marine
- 841 Science, 6, https://doi.org/10.3389/fmars.2019.00139, 2019.
- 842 Su, J., Dai, M., He, B., Wang, L., Gan, J., Guo, X., Zhao, H., and Yu, F.: Tracing the
- origin of the oxygen-consuming organic matter in the hypoxic zone in a large eutrophic
- estuary: the lower reach of the Pearl River Estuary, China, Biogeosciences, 14, 4085-
- 845 4099, https://doi.org/10.5194/bg-14-4085-2017, 2017.
- 846 Syvitski, J. P. M. and Kettner, A.: Sediment flux and the Anthropocene, Philosophical
- Transactions of the Royal Society A: Mathematical, Physical and Engineering Sciences,
- 848 369, 957-975, https://doi.org/10.1098/rsta.2010.0329, 2011.
- Wang, B., Hu, J., Li, S., and Liu, D.: A numerical analysis of biogeochemical controls
- 850 with physical modulation on hypoxia during summer in the Pearl River estuary,
- Biogeosciences, 14, 2979-2999, https://doi.org/10.5194/bg-14-2979-2017, 2017.
- Wang, B., Hu, J., Li, S., Yu, L., and Huang, J.: Impacts of anthropogenic inputs on

- hypoxia and oxygen dynamics in the Pearl River estuary, Biogeosciences, 15, 6105-
- 854 6125, https://doi.org/10.5194/bg-15-6105-2018, 2018.
- Wang, G., Cao, W., Yang, Y., Zhou, W., Liu, S., and Yang, D.: Variations in light
- 856 absorption properties during a phytoplankton bloom in the Pearl River estuary,
- 857 Continental Shelf Research, 30, 1085-1094,
- 858 https://doi.org/10.1016/j.envres.2021.111579, 2010.
- 859 Wang, H., Dai, M., Liu, J., Kao, S.-J., Zhang, C., Cai, W.-J., Wang, G., Qian, W., Zhao,
- 860 M., and Sun, Z.: Eutrophication-Driven Hypoxia in the East China Sea off the
- 861 Changiang Estuary, Environmental Science & Technology, 50, 2255-2263,
- 862 https://doi.org/10.1021/acs.est.5b06211, 2016.
- Wang, J. J., Bouwman, A. F., Liu, X. C., Beusen, A. H. W., Van Dingenen, R., Dentener,
- 864 F., Yao, Y. L., Glibert, P. M., Ran, X. B., Yao, Q. Z., Xu, B. C., Yu, R. C., Middelburg,
- J. J., and Yu, Z. G.: Harmful Algal Blooms in Chinese Coastal Waters Will Persist Due
- 866 to Perturbed Nutrient Ratios, ENVIRONMENTAL SCIENCE & TECHNOLOGY
- 867 LETTERS, 8, 276-284, https://doi.org/10.1021/acs.estlett.1c00012, 2021.
- 868 Wang, K., Chen, J., Jin, H., Li, H., Gao, S., Xu, J., Lu, Y., Huang, D., Hao, Q., and
- 869 Weng, H.: Summer nutrient dynamics and biological carbon uptake rate in the
- 870 Changjiang River plume inferred using a three end-member mixing model, Continental
- 871 Shelf Research, 91, 192-200, https://doi.org/10.1016/j.csr.2014.09.013, 2014.
- Wang, Y., Wu, H., Lin, J., Zhu, J., Zhang, W., and Li, C.: Phytoplankton Blooms off a
- 873 High Turbidity Estuary: A Case Study in the Changjiang River Estuary, Journal of
- 874 Geophysical Research: Oceans, 124, 8036-8059, https://doi.org/10.1029/2019jc015343,
- 875 2019.
- 876 Wen, G., Liang, Z., Xu, X., Cao, R., Wan, Q., Ji, G., Lin, W., Wang, J., Yang, J., and
- 877 Huang, T.: Inactivation of fungal spores in water using ozone: Kinetics, influencing
- 878 factors and mechanisms, Water Research, 185, 116218,
- 879 https://doi.org/10.1016/j.watres.2020.116218, 2020.
- 880 Wu, C. S., Yang, S., Huang, S., and Mu, J.: Delta changes in the Pearl River estuary and
- its response to human activities (1954–2008), Quaternary International, 392, 147-154,
- 882 https://doi.org/10.1016/j.quaint.2015.04.009, 2016.
- Yang, H., Wang, T., Yang, D., Yan, Z., Wu, J., and Lei, H.: Runoff and sediment effect
- of the soil-water conservation measures in a typical river basin of the Loess Plateau.
- 885 CATENA, 243, 108218, https://doi.org/10.1016/j.catena.2024.108218, 2024.
- 886 Yu, L., Gan, J., 2022. Reversing impact of phytoplankton phosphorus limitation on
- coastal hypoxia due to interacting changes in surface production and shoreward bottom
- 888 oxygen influx. Water Res. 118094 https://doi.org/10.1016/j. watres.2022.118094.
- Yu, L., Fennel, K., Laurent, A., 2015. A modeling study of physical controls on hypoxia
- generation in the northern Gulf of Mexico. J. Geophys. Res. Oceans 120, 5019–5039.
- 891 https://doi.org/10.1002/2014JC010634.
- 892 Yu, L., Gan, J., Dai, M., Hui, C., Lu, Z., Li, D., 2020. Modeling the role of riverine
- 893 organic matter in hypoxia formation within the coastal transition zone off the Pearl
- 894 River Estuary. Limnol. Oceanogr. 9999, 1–17. https://doi.org/10.1002/lno.11616

- 895 Zhang, S., Lu, X. X., Higgitt, D. L., Chen, C.-T. A., Han, J., and Sun, H.: Recent
- 896 changes of water discharge and sediment load in the Zhujiang (Pearl River) Basin,
- 897 China, Global and Planetary Change, 60, 365-380,
- 898 https://doi.org/10.1016/j.gloplacha.2007.04.003, 2008.
- 899 Zhang, Z., Wang, B., Li, S., Huang, J., and Hu, J.: On the Intra-annual Variation of
- 900 Dissolved Oxygen Dynamics and Hypoxia Development in the Pearl River Estuary,
- 901 Estuaries and Coasts, 45, 1305-1323, https://doi.org/10.1007/s12237-021-01022-0,
- 902 2022.

903